United States Geological Survey National Earthquake Hazards Reduction Program

Final Technical Report
September 21, 2009

Paleoseismological characterization of earthquakes and a geologic slip rate at Parkfield, CA

NEHRP External Grant Number
07HQGR0094

Principal Investigator: J Ramón Arrowsmith (ramon.arrowsmith@asu.edu)
School of Earth and Space Exploration
Arizona State University Box 1404
Tempe, AZ 85287-1404
Office Phone: (480) 965-3541
Fax: (480) 965-8102

Ph.D. Student: Nathan A. Toké (nathan.toke@asu.edu)

Summary:
The purpose of this investigation was to characterize the rate, style, and distribution of late Holocene slip along the Parkfield segment of the San Andreas Fault (SAF). Herein, we present results from three new paleoseismic trenches at the Miller's Field paleoseismic site along the main SAF surface trace at Parkfield, we discuss the site's geomorphology, deformation record, estimate a late Holocene slip rate from an offset channel at this site, and present the information about an unsuccessful pilot study of paleoseismology along the Southwest Fracture Zone.

Abstract

In October 2007, we investigated three new trenches at the Miller's Field paleoseismic site along the San Andreas Fault at Parkfield, CA. This effort followed our 2004 paleoseismic campaign, prior to the ~Mw 6 Parkfield earthquake. We also opened 5 exploratory trenches along the Southwest Fracture Zone (SWFZ). The SWFZ trenches were located on the Ranchita Canyon alluvial fan which displays tectonic warping and a vegetation lineament; however, no interpretable stratigraphy was exposed indicating a low rate of deposition relative to bioturbation.

The Miller's Field site deformed Holocene terrace constructed of overbank deposits of sand and silt and a sag pond that developed across a ~10 m right step in the surface trace of the SAF. Importantly, a channel is offset across the sag pond's scarp. The sag is filled by alternating layers of sandy clay and dark layers of silty clay that onlap the scarp. Deformation is spread across the sag. Faults are thin clay bands that offset the stratigraphy without clear upward terminations. The 2004 earthquake ruptured this site with overlapping, left stepping, en-echelon cracks. Most of these cracks opened <5cm. We infer that these cracks heal by infilling with silt and clay forming oblique (to the SAF trend) linear clay bands within the subsurface. Thus, the oblique clay shear band structures observed here represent many cycles of deformation from creep and ~ M6 earthquakes. No evidence of larger surface ruptures such as large filled fissures or colluvial wedges could be confidently discerned.

Radiocarbon ages suggest the sag began to form after 890 A.D.; apparently, formation of the sag's scarp initiated the incision of a channel across from a larger, previously-beheaded, channel which focused erosion across the fault. Since then the channel was offset 18.5-23.0 m. Thus, we use probability density function (PDF) analyses with age bracketing of the sag to estimate a slip rate for the main trace of the SAF. The PDF analyses suggests the slip rate is most likely between 25-30 mm/yr with a preferred estimate of 26.1 (+8/-7) mm/yr. While this range includes 33 mm/yr, the upper part of the range is skewed by the oldest radiocarbon age within the sag which is >20 cm above the base of the sag and above a sandy unit; indicating the channel had already initiatied. A 25-30 mm/yr slip rate is low relative to some GPS inversions for slip below the SAF seismogenic zone and geologic slip rates measured along the SAF in the Carrizo Plain 100 km southeast. However, it is consistent with local observations of historical slip from creep and M6 earthquakes. These data imply that recent SAF behavior which has attracted earthquake scientists to Parkfield has persisted over millennia and significant slip may be accommodated by structures in the wider aperture of the SAF zone.

Table of Contents

ABSTRACT **2**

TABLE OF CONTENTS **3**

LIST OF TABLES 3
LIST OF FIGURES 3

INTRODUCTION **4**

SITE SELECTION AND METHODS **6**

SOUTHWEST FRACTURE ZONE EXPLORATION (SWFZ) **8**

2007 MILLER'S FIELD PALEOSEISMOLOGY **9**

MILLER SAG TRENCH 2007 (MST 07) 9
PRESSURE RIDGE TRENCH 2007 (PT 07) 11
SUMMARY OF DEFORMATION STYLE 13

ESTIMATING A LATE HOLOCENE SLIP RATE **14**

TERRACE DEFORMATION AND OFFSET MEASUREMENT 14
PROBABILITY DENSITY FUNCTION (PDF) SLIP RATE ANALYSES 16

DISCUSSION AND RECOMMENDATIONS **17**

ACKNOWLEDGEMENTS **19**

PUBLICATIONS AND PRESENTATIONS: **19**

REFERENCES **20**

LIST OF TABLES

TABLE 1. MST radiocarbon data 23
TABLE 2. PT radiocarbon data 24

LIST OF FIGURES

FIGURE 1. Location of the Parkfield segment 25
FIGURE 2. Southwest fracture zone pilot study 26
FIGURE 3. Miller's Field Paleoseismic site map 27
FIGURE 4. MST 2007 logs 28
FIGURE 5. PT 2007 logs 29
FIGURE 6. Offset measurement 30
FIGURE 7. Slip Rate Probability Density Functions 31

Introduction

Historically, the Parkfield segment of the San Andreas Fault (SAF) has represented a transition in fault behavior where both aseismic fault creep and six moderate magnitude (~M6) surface-rupturing earthquakes have occurred (figure 1; e.g., Toke and Arrowsmith, 2006). Toke and Arrowsmith, following previous studies (e.g., Sieh and Jahns, 1984; Segall and Harris, 1986; Harris and Archuleta, 1988; Arrowsmith et al., 1997), showed that a slip deficit is accumulating along the Parkfield segment since the ~M8 1857 Fort Tejón Earthquake (the last Great southern SAF earthquake). The slip deficit is nearly 5 meters at the southeastern end of the segment and diminishes to zero 30 km northwest of Cholame, CA (e.g., Toke and Arrowsmith, 2006). The distribution of the calculated slip deficit is controlled by the geodetically-measured rate of aseismic fault creep which decreases from >25 mm/yr in the northwest to 0 mm/yr near highway 46 at the Cholame segment in the southeast (e.g., Murray et al., 2001; Murray and Langbien, 2006; Titus et al., 2005; and Titus et al., 2006) and from slip in historical moderate magnitude earthquakes (e.g., Lienkaemper and Prescott 1990 and Lienkaemper et al., 2006). These mechanisms of strain release are balanced strain accumulation which is assumed to be ~33 mm/yr as suggested by far field geodetic observations and measured at several geologic sites in the Carrizo segment of the SAF (e.g., Sieh and Jahns, 1984, Noriega et al., 2006, and Meade and Hager, 2005). The existence of a historical slip deficit extending into the Parkfield segment leads to two hypotheses about SAF slip near Parkfield.

1) ***The Parkfield segment may be subject to temporal changes in strain release rate*** such that the slip deficit could be balanced by infrequent large earthquakes extending into the Parkfield segment, a change in the distribution and rate of aseismic fault creep, or frequency of moderate magnitude earthquakes.

2) ***Slip along the SAF at Parkfield may be significantly distributed along structures parallel to the main trace of the fault*** such as the Southwest Fracture Zone (SWFZ) and White Canyon Faults (figure 1) and thus previous slip budgets overestimate the slip rate for the main trace of the SAF.

In 2004, prior to the latest Parkfield earthquake, we excavated and logged two paleoseismic trenches at the Miller's Field Paleoseismic Site (Toke et al., 2006). A trench across a sag pond (MST04) and another across a pressure ridge (PT04) along the main SAF trace revealed more than 3000 years of fault zone stratigraphy. Both trenches presented tectonic deformation structures that were consistent with surface deformation from moderate magnitude earthquakes and aseismic creep. However, the data did not preclude the possibility of larger surface rupturing earthquakes at Parkfield. In our 2007 investigation, we revisited the Miller's Field paleoseismic site (figure 2) to further assess the 2004 results, to better date the site's stratigraphy, and to estimate a slip rate for a right-laterally offset stream channel at the Miller's Field sag pond (figures 3-7). In addition to the main SAF, we were also interested in investigating the slip history of the southwest fracture zone (SWFZ; figure 2). Because of the SWFZ's slip during recent moderate magnitude Parkfield earthquakes (e.g., Rymer et al., 2006; Lienkaemper et al., 2006; and Lienkaemper and Prescott, 1989) and its prominent tectonic geomorphology (figure 1) it may reveal valuable information about SAF fault zone mechanics and rupture history. Unfortunately, our 2007 trenches along the SWFZ did not yield interpretable stratigraphy (figure 2).

In this report we present the results from three new paleoseismic excavations at the Miller's Field Paleoseismic Site, new radiocarbon results from our 2004 and 2007 excavations, and geomorphic observations that suggest there have been no large ground ruptures at Parkfield for the past ~1000 years. Additionally, we use probability density function analyses to explore the range of possibilities for the age of formation and total right-lateral offset for a channel at this paleoseismic site. From these data, we interpret a late Holocene slip-rate for the main trace of the SAF at Parkfield which appears to be less than the often cited SAF slip rate of 33 mm/yr for the south-central San Andreas Fault (e.g., Sieh and Jahns, 1984 and Meade and Hager, 2005). The results presented herein support hypothesis 2 outlined above; therefore we conclude the report by discussing implications for earthquake hazard and fault zone mechanics from the results of a relatively low slip rate for the main trace of the SAF at Parkfield with no evidence for recent large earthquakes along the segment.

Site Selection and Methods

Using the B4 San Andreas Fault LiDAR (e.g. Bevis et al., 2005) and Google Earth imagery, we remotely mapped tectonic geomorphology and identified potential sites for paleoseismic and slip rate investigation on the main SAF at Parkfield (figure 1; Toke and Arrowsmith, 2007 and Toke and Arrowsmith, in progress). For the SWFZ, we identified paleoseismic sites using lineaments identified with Google Earth and DOQQ imagery. From our initial mapping we selected three slip rate sites of interest along the main SAF (Miller's Field, Turkey Flat, and Gold Hill Terrace) and broader region of interest for paleoseismic exploration on the SWFZ southeast of the Miller's Vineyard (figure 1). Much of the southeastern part of Cholame Valley is owned by the Hearst Corporation. Unfortunately, with so much geological work ongoing in the Parkfield area they were not interested in starting another project on their Ranch over the time span of this investigation. This eliminated the Gold Hill Terrace Site as an option. The Turkey Flat Site is a very large (>600 meter) offset stream channel of the SAF which will require more people power and a greater excavation and geochronology budget to properly measure a slip rate at the site. Therefore, we decided to build upon our knowledge of the Miller's Field paleoseismic site and measure a slip rate from the small offset stream channel across the sag pond (figure 3) and to explore the SWFZ (figure 2). Unfortunately, the SWFZ site was not stratigraphically well-suited for paleoseismic investigation.

At the Miller's Field Site, we excavated 4 trenches with the help of Bob's Backhoe of Parkfield. We opened two fault normal trenches across the Miller's Sag (MST07 and MST07c) and one fault parallel trench (MST07parallel) across the upstream thalweg of the small right-laterally offset channel that crosses the SAF at the Miller's Sag (Figures 2 and 7). MST07c was located at the position of greatest surface deformation after the 2004 surface rupture. Unfortunately, because of elevated groundwater levels in 2007 we could not keep all three 2007 MST trenches dry enough to prevent collapse. MST07c collapsed and was not logged.

MST07parallel spanned the topographic depression of the offset stream channel and crossed the northeast corners of both MST07 and the MST04 trenches. MST07parallel was dug with the purpose of linking stratigraphy between the 2004 and

2007 excavations and to search for any channel deposits associated with the right-laterally offset channel (figure 3). Additionally, we excavated one fault-normal trench across a relatively-dry portion the Miller's Field pressure ridge scarp (PT07; figure 6). The purpose of this trench location was to test for consistency of deformation history with PT04 and search for records of larger surface rupturing events in the older stratigraphy exposed along the Pressure Ridge.

We constructed meter-scale line grids for all three paleoseismic trenches and logged them on metric graph paper at 1:20 scale. Paleoseismic logs were redrafted onto Mylar and scanned. Trench walls were photographed and rectified. Stratigraphic units and charcoal radiocarbon samples were flagged using painted nails. Radiocarbon samples were collected in aluminum foil and placed in labeled plastic bags.

In 2007, we resurveyed the area of the 2004 Total Station survey of the Miller's Field site (Toke et al., 2006). These surveys were at a variable shot spacing ranging from 5 m farther from the fault to about 10 cm within the surface trace's fault zone. Herein we utilize these surveys to depict the trench locations accurately over the 2005 B4 LiDAR data. Additionally, we used a 0.5 m digital elevation model (DEM) derived from the B4 LiDAR to measure the displacement of the right-laterally offset channel at the Miller's field sag pond and help estimate a slip rate.

Charcoal samples from our 2007 trenches and samples from the 2004 trenches were sent to University of California, Irvine W. M. Keck Carbon Cycle Accelerator Mass Spectrometry Laboratory (UCI-KCCAMS) for analyses; adding to our previously results from Toke et al., 2006; tables 1-2. Twenty samples were covered via a Southern California Earthquake Center geochronology award, significantly leveraging the original USGS NEHRP award. These dates are combined with dates from Toke et al., 2006 to determine the ages of the exposed Holocene stratigraphy, the timing of deformation, and age of channel incision and offset. Finally, we use probability density function analyses to infer a slip rate for the main trace of the SAF.

Southwest Fracture Zone Exploration (SWFZ)

On October 12, 2007 we opened one 30 meter and four 5 meter fault-perpendicular trenches to a depth greater than 1 meter across the SWFZ where it cuts the Ranchita Canyon alluvial fan (Figures 1 and 3). This portion of the SWFZ is delineated by a curiously wide vegetation lineament, a subtle northeast facing scarp, and surface fracturing that occurred in both the 1966 and 2004 Parkfield Earthquakes (Lienkaemper and Prescott, 1989 and Rymer et al., 2006; figure 3). An ephemeral channel is incised into the Ranchita Canyon fan and merges east with the Little Cholame Creek. This ephemeral stream is incised ~2 meters into the fan and exposes approximately 1 meter of alluvial stratigraphy consisting of deposits of silt, sand, and angular gravel. This upper stratigraphy overlies a heavily bioturbated and structureless unit of sand and silt. Unfortunately we learned that the interpretable stratigraphy was only preserved along the southeastern bank of the stream and here the deformation by the SWFZ was obscured by a row of oak trees and their roots that line the stream bank.

The 30 meter SWFZ-perpendicular trench was dug 1.5 meters deep and just over 1 meter wide. Backhoe workers extended the trench from 5 meters up fan of the subtle SWFZ scarp to ~25 meters down fan from the scarp into the wide vegetation lineament. However, the trench revealed only massive bioturbated sand and gravel across both sides of the exposure (figure 2c). We then moved ~10 meters down fan, but along the same trend (figure 2b, exploratory trench A) to see if the stratigraphy was better there. It was not. Next, we moved southeast of the vegetation lineament and dug exploratory trench B perpendicular to the SWFZ, but only 5 meters long and just over 1 meter deep. Again no stratigraphy was observed. Exploratory trenches C and D were also about 5 meters long, but located to the northwest of the Ranchita Canyon Creek along the SWFZ (figure 2). These test pits also revealed no stratigraphy. These SWFZ trenches were closed after it was apparent that there was no stratigraphy or tectonic structures to interpret.

Apparently, the stratigraphy of the Ranchita Canyon Fan is poorly preserved. This may be attributed to bioturbation of the relatively fine fan deposits. Despite their small size, the plants of this vegetation lineament have very large diameter roots (2-6 cm) that extend to depths of greater than 1 meter. It is also likely that the Ranchita Canyon stream

has not migrated very much in it's recent past given the occurrence of large oak trees along its banks. Given our results it seems likely that the sediment supply for the Ranchita Canyon fan is far slower than its rate of bioturbation. Also, it appears that the surface slip at this location is dispersed over a >20 meter aperture with creep and small surface ruptures. This deformation zone is probably attractive to biota and may aid in degradation of the fan stratigraphy. Given these results, the best candidates for future SWFZ investigations would be sites with younger and faster sedimentation and perhaps a narrower geomorphic lineament. Paleoseismic site selection will require detailed geomorphic mapping of the SWFZ. Unfortunately, the SWFZ was not imaged by the B4 LiDAR project (e.g. Bevis et al., 2005) and thus future studies will require new imaging or intensive field mapping.

2007 Miller's Field Paleoseismology

The 2007 paleoseismic trenches exposed the same stratigraphic sequences as documented in detail in Toke et al., 2006 (figures 4-5) and provided new radiocarbon samples to better constrain the timing of deposition and deformation (tables 1-2). The MST07 trench revealed that stratigraphic units are contiguous across the sag pond fault zones 1-3 (which was unclear in the 2004 excavations; figure 4). This was important because it allowed us to better interpret the radiocarbon age results, determine which ages contained detrital (inherited) signatures, and constrain the timing of sag pond formation. Moreover, the 2007 trenches documented a pattern of structures consistent with the 2004 trenches and deformation from creep and moderate magnitude earthquakes.

Miller Sag Trench 2007 (MST 07)

MST 07 was located at the southeastern end of the Miller's Field sag pond (figure 3). This trench was sited close to MST 04 (Toke et al., 2006) and connected with MST07parallel to link the stratigraphic relationships and test if the upstream section of the offset channel was associated with channel fill deposits. The fluvial terrace and sag pond fill stratigraphy exposed in MST 07 (figure 4) is correlative to MST 04 and through

reinvestigation and new radiocarbon analyses we learned new information about stratigraphic correlations across the MST fault zones as well as more about the deformation structures exposed in both trenches.

The MST 07 sag fill deposits overly fluvial deposits of the Little Cholame Creek. To the northeast of fault zone 1 (FZ1; figure 4) these once tabular units are down warped by the SAF deformation (MSE-102 through MSE 108). In MST 07 the MSE-102 unit is a coarse sand and correlative to the unit MSE2 in the MST 04 exposures. In those exposures, this unit consisted of numerous filled channel deposits that may represent a former location of the Little Cholame Creek. This unit is overlain by clayey sandy silt (MSE-103) and a buried organic-rich soil horizon (MSE-104). MSE-104 is warped downward below the trench exposure and overlain by a thick (about one meter) sequence of sands (MSE-105 through MSE-107). The sequence of sands forms an angular unconformity with MSE-104; suggesting that the MSE-104 surface was not flat lying when this overbank sequence was deposited. These units are overlain by another buried organic-rich soil horizon (MSE-108). This horizon merges with the present day root and till horizon east of FZ1 and is warped down within the fault zone.

MSE-108 is offset across FZ1. West of the fault MSE-108 becomes thicker. This thickening likely represents progressive dip slip deformation at a rate comparable to soil creep and formation. MSE-108 contains three thin deposits of charcoal and clay (charcoal stringers) that appear to have been deposited over a progressively sloping surface. This indicates that the sag pond's scarp was actively increasing slope as the soil horizon was developing. A radiocarbon analysis of charcoal from the lowermost charcoal stringer yielded an age of 890-1040 A.D. (table 1), this is the oldest bounding age for the sag pond. MSE-108 is overlain by a sequence of sag fill deposits that on-lap against the sag pond's eastern scarp (MSE-109 through MSE-119; figure 4). The lower section of the sag filling sequence (MSE-109 through MSE-115) spreads across the width of the sag pond exposure and consists of relatively thinly bedded deposits (figure 4) alternating between dark organic-rich clayey soil horizons and deposits of sandy silt. Radiocarbon ages suggest that this half a meter thick sequence of sag stratigraphy was deposited from 1400-1500 A.D., whereas the upper sag units (MSE-116 through MSE-119) are located between FZ3-FZ4 and fill roughly 1.5 meters in the last 500 years. The earlier period

rapid sag filling could be linked to climate perturbations, pulses of increased slip rate (and thus scarp erosion), or linkage with a significant source of sediment delivery to the sag pond; such as the right-laterally offset stream channel (figures 3 and 6).

To the west of fault zone 4 (FZ4), the MST 07 trench exposed MSW 104 through MSW-108. MSW-105 is a buried and warped soil horizon, probably correlative in age to the sequence of MSE-104 through MSE-108 (figure 4). MSW-106 is silty sand that was deposited and preserved over the MSW-105 soil horizon. A radiocarbon sample suggests that MSW106 was deposited synchronously with the middle-upper sag deposits (1440-1630 A.D.) and faulted into place. Units MSW-107 and MSW-108 overly the other western terrace deposits and the deformed sag fill deposits near FZ4. These overlying units are faulted, but have clearly experienced relatively little deformation.

Deformation structures are distributed across the MST 07 exposure and the same four fault zone localizations (FZ1-FZ4) were seen in MST 04 (figures 3-4; Toke et al., 2006). Faults are delineated by sub-vertical to vertical clay bands (clay shear bands) that extend to the root and till zone of the MST stratigraphy; many of which show apparent horizontal and vertical offsets. While there is clearly long-lived slip on FZ1, the most apparent offset is accommodated by FZ3 and FZ4; the depocenter of sag pond fill. FZ4 was also the most active strand of the 2004 surface rupture (figures 3 and 6, black lines) which was manifest as left-stepping enechelon, overlapping, opening-mode surface cracks that were oblique to the trend of the SAF (Toke et al., 2006 and Rymer et al., 2006). Cracks were 0.5-10.0 meters long, opened several centimeters, with cm-scale right lateral offset. We suspect that these cracks filled with fine material from the processes of diffusion, aeolian deposition, and overland flow and then healed from shrink/swelling events within the clay-rich terrace soils. Importantly, the majority of fault surfaces observed within the MST and PT trenches were oblique the SAF structures. In fact, portions of the MST 07 trench repeatedly failed along these clay shear bands and failure surfaces are readily observed in the MSE 07se photolog (figure 4b).

Pressure Ridge Trench 2007 (PT 07)

The PT 07 trench was located about 70 m northwest of PT 04 along the pressure ridge southeast of the sag pond (figure 3). This site was a prominent zone of surface

fracturing in the 2004 Parkfield earthquake. This part of the pressure ridge is less vegetated than the PT 04 site. Thus we hypothesized it would have less bioturbation and pedogenic alteration of the fault zone stratigraphy. Additionally, we targeted the pressure ridge scarp as a site where we would expect significant vertical deformation that would likely be preserved from a large ground rupture.

The PT 07 fluvial terrace stratigraphy and deformation structures were consistent between trench walls (figure 5) and the PT 04 trench (Toke et al., 2006). Ten new radiocarbon ages were combined with the previous four ages to better constrain the timing of fluvial deposition (table 2). The additional samples allowed us to determine that at least three of the previous samples had a significant transport history prior to deposition and thus the ages are detrital and not useful in constraining the ages of the exposed stratigraphy. With only 14 total radiocarbon analyses it is likely that some of the ages reported here may still be significantly older than their host stratigraphy.

The oldest stratigraphic unit exposed in PT 07 is PTE-033 (a clean sand; 1880-1690 B.C.; figure 5 and table 2). This unit is overlain by an alternating sequence of two thin clay units and clean overbank sands (PTE-034-PTE037). This sequence of stratigraphy was cut by small channels which are now filled with small pebbles and sand. The size of these channels and their deposits is smaller than that of the current Little Cholame Creek and probably represents cutting of the terrace stratigraphy by a smaller stream such as the currently-beheaded channel downstream of the sag pond (figure 3).

The PTE-033 to PTE-037 sand and clay sequence is overlain by the tabular clayey silt (PTE-038) and an organic-rich, dark, buried soil horizon (PTE-039). PTE-039 is correlative with unit PTE-11 in the PT04 trench, however, it is a much thinner horizon there (Toke et al., 2006). Above PTE-039 the terrace stratigraphy extends for more than four meters vertically with alternating silty and clayey sands separated by thin clay rich horizons with significant amounts of charcoal (charcoal stringers). Previously (Toke et al., 2006), we naively inferred that these clayey charcoal stringers represented *in-situ* terrace burn surfaces. However, additional radiocarbon ages have shown that many of these charcoal pieces have significant transport histories and thus these horizons can not be *in-situ* burns. Now we interpret them to be charcoal that floated out of suspension at the

waning stages of paleofloods; which explains why they are associated with thin horizons of clay and silt within the terrace stratigraphy.

The youngest age (680-540 B.C.) within the terrace stratigraphy on the east side of the SAF comes from PTE048 (more than a meter below the current ground surface; figure 5). One the west side of the fault only one radiocarbon sample has been successfully analyzed; yielding an age of 640-770 A.D. This age comes from the lowest of four tabular terrace units on the west side of the fault and nearly two meters below the present day land surface. Thus, the vertical offset across this part of the pressure ridge is at least five meters, but could be more.

The primary SAF zone exposed in PT 07 is about two meters wide, however some cracking was also observed in the stratigraphy east of the primary fault zone. Offsets show apparent vertical displacement, but changes in unit thicknesses across individual faults and some pop up structures (especially PTE-039) suggest significant right lateral displacement and oblique complexities. Interestingly, the stratigraphy east of the SAF is tilted so that it dips northeast, while units to the west of the SAF are nearly horizontal. This suggests that the SAF must bend to the east or begin to dip more eastward in the shallow subsurface. This is inconsistent with the observation of southwest dipping fault splays which merge to a narrower slip surface near the base of the trench.

Within the PT 07 fault zone there is significant reworking of units and nearly all fault splays (clay shear bands) reach the surface of the trench. However, in PT 04 we found a small, discontinuous, layer (probably a small colluvial deposit; PTFZ-005) containing charcoal and leaves within the fault zone. Radiocarbon analysis indicated an age of 1240-1400 A.D. for this deposit (table 2). Apparently, the pressure ridge scarp had begun to form by this time. Despite this relatively small colluvial deposit, we did not observe evidence of large colluvial deposits that one would expect to preserve with significant vertical offset in large ground rupturing earthquakes.

Summary of deformation style

We observed no evidence of filled fissures or significant colluvial scarp deposits that would be indicative of discrete large ground rupturing earthquakes. Nearly all fault surfaces are clay shear band surfaces that are oblique to the trend of the SAF trace. These

clay shear bands appear to form from left-stepping moderate magnitude surface cracks that fill with fine material and heal. These faults are distributed widely across the fault zone indicating there have been many generations of moderate magnitude surface ruptures. Additionally, most faults extend to the surface of the trench exposures which suggests that they are reactivated in aseismic slip events or subsequent moderate magnitude events. Finally, it appears that post-1630 deposits overly FZ4 in the MST 07 exposure. This deposit is faulted, but shows no signs of experiencing significant ground rupture. Thus, we interpret that the deformation structures exposed within the Miller's Field paleoseismic trenches are formed by small surface ruptures from moderate magnitude earthquakes and aseismic creep and not large ground rupturing earthquakes. While it is still plausible that ruptures from large earthquakes, such as 1857 (e.g. Sieh, 1978a and 1978b) extend into the Parkfield segment. It appears that slip and ground rupture must decay rapidly along the Parkfield segment such that these ruptures are indistinguishable from moderate magnitude ruptures 20 km northwest of the Cholame segment (figure 1). This is consistent with the observation of a SAF slip deficit that decays to the northwest across the Parkfield segment (e.g., Toke et al., 2006) and our estimates of a late Holocene slip rate (below).

Estimating a late Holocene slip rate

Terrace Deformation and Offset Measurement

The MST-07parallel trench was cut across the small topographically-incised channel at the southeast corner of the sag pond and about 4 meters northeast of the sag pond's scarp (figures 3 and 6). The purpose of this trench was to link the stratigraphy exposed in MST-07 to MST-04 (figure 4 and Toke et al., 2006) and to determine if there were any channel deposits that could be correlated between the sag pond's offset channel (figures 3 and 6). The MST-07parallel trench exposed the tabular units MSE102-MSE104 (formerly referred to as MSE 2-MSE 4 in Toke et al., 2006) between MST-07 and MST-04, thus linking the stratigraphic records.

Unsurprisingly, the exposure of units MSE103 and MSE104 (thick Little Cholame Creek overbank deposits of clayey sand and silt with pedogenic alteration) were not cut by channel deposits. Thus, the upstream portion of the offset channel is merely a topographic depression. The downstream portion of the offset channel (on the west side of the SAF/sag pond) is deeper, wider, and has several steps in its bed which expose discrete channel fill deposits of pebbles and small gravels. This indicates that the downstream channel was once connected to a substantial watershed capable of sourcing and transporting such material. Thus, this beheaded channel has been offset along the fault for significantly more than the apparent ~20 m offset across the sag pond. However, the topographically incised channel on the upstream side of the sag pond must have been driven by focused erosion at this site and therefore is linked to the downstream channel. The most likely way to focus such erosion is to create a local drop in base-level combined with a sediment evacuation route. Here the local drop in base level was the formation of the northeast side up fault scarp along the pressure ridge and extending along the sag. With the older beheaded channel across the fault scarp it provided a sediment evacuation route to focus erosion during surface runoff. Thus, the upstream topographic channel, offset ~20 m, was likely driven by focused erosion when the downstream channel was directly across the fault (figures 3 and 6).

One could argue that the sag pond its self could create enough of a base level drop and mechanism to focus erosion and form the upstream channel; thus negating the idea of linking this offset channel pair. However, if this were the case, then we still must consider where the beheaded channel was located. If the sag pond formed while the beheaded channel was still to the southeast (along the emerging pressure ridge) we would expect that the beheaded channel would have driven a wave of incision up the pressure ridge scarp and a second channel would have been preserved. A second channel does not exist and therefore the offset channel pair at the Miller's sag represents the opportunity to measure a maximum slip rate for the main trace of the SAF at Parkfield. Moreover, at this site the timing of fault scarp development is recorded by the formation of the sag pond and thus by determining the age of the sag pond we also can determine the age of topographic incision and estimate the slip rate (figure 7).

Probability Density Function (PDF) Slip Rate Analyses

We could simply propagate the errors in age and offset to estimate a slip rate, but our estimates are not unique, and the errors are not symmetric, or well fit by a normal distribution, so we chose to follow the approach suggested by Sally McGill and others to use a simply joint probability approach to more accurately determine the slip rate PDFs. To precisely determine the amount of right-lateral offset across this topographically-linked channel pair we constructed fault-parallel upstream and downstream channel profiles (figure 6) using a 0.5 meter B4 LiDAR derived DEM (e.g., Bevis et al., 2005). From these profiles we measured right lateral offset using the present day channel thalwegs' positions. The downstream channel has two poorly defined thalwegs so we measure both a minimum offset of 18.5 meters and a maximum offset of 23 meters (figure 6b). Because this channel is subject to much bioturbation by feral pigs and farm activity, we assume that the PDF for this right lateral offset should be equally weighted with a peak probability at the median of 18.5 and 23 meters, forming a triangular PDF (figure 7a).

The timing of channel incision is linked to the formation of the sag pond/pressure ridge scarp. Therefore we use stratigraphic and age relationships of the sag pond filling units (MST 07; figure 4) and a small colluvial deposit exposed in PT 07 (figure 5; Toke et al., 2006) to constrain the age of channel incision. Three clay and charcoal horizons (charcoal stringers) at the base of the sag pond (within MSE-108) display progressively steeper slopes over what was the active terrace surface (figure 4). These relationships suggest that a scarp was forming during their deposition. Radiocarbon analysis of the lower charcoal stringer within MSE-108 suggests that the overlying sag pond deposits post date 890-1040 A.D. (figure 4 and table 1). Direct stratigraphic evidence that the upstream side of the offset channel had incised is unit MSE-111 (1410-1450 A.D.; figure 4 and table 1) which is a sandy sag fill of reworked terrace material. Such a fill could not form until the upstream channel had incised to a depth greater than the organic-rich soil horizon. Thus we know that channel incision occurred between MSE-108 and MSE-111. Using this knowledge we construct a conservative PDF for the age of channel formation (blue curve; figure 7b). This PDF assumes equal probability for time of channel incision between maximum and minimum radiocarbon ages of MSE-108 and MSE-111; forming

a plateau-shaped PDF. Combining this PDF with the right-lateral offset PDF results in a broad slip rate PDF (blue curve; figure 7c) with a mean rate of 24.5 (+12/-7) mm/yr.

The presence of the sand MSE-111 unit is stronger evidence for the channel than the interpretation of a small topographic warping (MSE-108). However, to deposit this sandy material the channel must have already eroded through the ~ 10cm thick dark organic-rich soil horizon of the terrace; indicating that the age of MSE-111 is younger than the age of the channel. To refine the PDF slip rate estimation we use some information from the PT trenches (figure 5 and Toke et al., 2006). Within the PT fault zone we observed a small colluvial deposit with datable material. Radiocarbon analysis indicated that this scarp-derived deposit (PTFZ-005) was formed between 1250 and 1390 A.D.; significantly prior to MSE-111. Formation of a scarp derived deposit suggests that the entire pressure ridge-sag feature had formed by this time. We use this age to form a refined, but still conservative PDF for age of channel formation (black curve; figure 7b). This PDF simply assumes that peak probability for age of channel formation is age of deposition of the PT colluvial deposit, forming a triangular PDF. The resulting slip rate PDF indicates a mean rate of 26.1 (+8/-7) mm/yr (black curve; figure 7c). By assuming that the incision of the offset channel occurred between the age of the PT colluvial deposit and the age of MSE-111 then we construct a less conservative slip rate estimate (figure 7b and 7c; red curves). This PDF suggests a mean slip rate of 28.8 (+6/-5) mm/yr.

Discussion and Recommendations

These PDF slip rate analyses do not preclude the possibility of a slip rate near the 33 mm/yr that has been measured for the SAF in the Carrizo Plain (e.g., Noriega et al., 2006). However, these analyses suggest it is likely that ***the slip rate at Parkfield is between 25 and 30 mm/yr for main trace of the SAF ~20 km northwest of the Cholame segment boundary***. This range is similar to a slip rate estimate by Sims, 1987 who estimated a rate of 26.3 (+3.9/-3.3) mm/yr in the southeastern Cholame Valley. Interestingly, near the Miller's Field site along the Parkfield segment the fault creeps at about 10 mm/yr (e.g., Lienkaemper and Prescott, 1989) and with the addition of slip from

moderate magnitude surface ruptures since 1857 (6 earthquake with 30-40 cm of slip) we calculate that main trace of the SAF has had a historical slip rate of about 22-26 mm/yr. This is comparable to the millennial-scale slip rates estimated herein. Additionally, all of the observations of the exposed deformation structures from four Miller's field paleoseismic trenches are consistent with deformation from the observed historical mechanisms of slip release (creep and moderate magnitude earthquakes). Taken together, ***these results imply that the SAF behavior that has attracted earthquake scientists to Parkfield over the past century has persisted over millennia*** and significant slip may be accommodated by structures in the wider aperture of the SAF zone such as the Southwest Fracture Zone, which also slipped in both the 1966 and 2004 Parkfield earthquakes (e.g., Lienkaemper and Prescott, 1989; Lienkaemper et al., 2006; and Rymer et al., 2006).

The remaining question is how is the 3-8 mm/yr of additional SAF zone slip accommodated. We do not yet have a slip rate for the Southwest Fracture Zone, but do know that it has accommodated significant slip in both the 1966 and 2004 earthquakes and displays prominent tectonic geomorphic features such as pressure ridges and deflected channels (e.g., Lienkaemper and Prescott, 1989; Lienkaemper et al., 2006; and Rymer et al., 2006). However, it seems unlikely that it has a slip rate of ~8 mm/yr. Platt and Becker, 2009 presented geodetic modeling, without imposing pre-existing faults, across the Pacific/North American plate boundary that suggests as much as 9 mm/yr of slip may be accommodated in the Salinian block of the California Coast Ranges. Thus, significant slip may be accommodated along structures such as the prominent Rinconada Fault (e.g., Jennings 1977). Additionally, Titus et al., 2005 observed that right-lateral slip rates increase from ~25 mm/yr over short apertures across the Creeping segment of the SAF to more than 30 mm/yr when aperture length was increased. Near Parkfield, another structure known as the White Canyon Fault (figure 1) displays a prominent geomorphic signature and appears to intersect with main SAF to the Cholame segment in the southeast. While, temporal changes in strain release rate could also account for these variations in slip release between SAF segments, ***we infer the variations in slip release are more likely due to slip being partitioned onto other active faults within the wider San Andreas Fault zone***. To test this hypothesis and investigate the possibility of increased seismic hazard along faults other than the main SAF, future studies should

target slip rate investigations of faults such as the Rinconada, White Canyon Fault, and the Southwest Fracture Zone. Additional slip rate estimations and paleoseismic studies along the more southeastern section of the SAF at Parkfield is warranted and may also shed light on this debate.

Acknowledgements

This research was also supported by the SCEC geochronology fund. We are thankful for participation by Mike Rymer, Angela Landgraf, Josh Coyan, Melanie Busch, David Haddad, and Alex Hanna. Additionally we thank the residents of Parkfield, the Miller Brothers, and Bob's Backhoe for their willingness to support our investigations.

Publications and Presentations

Publications (in preparation)

Toke, N.A., JR. Arrowsmith, M.J. Rymer, A. Landgraf, J. Coyan, M. Busch, and D. Haddad. "Long-lived creep, M6 earthquakes, and Holocene slip rate for the main trace of the San Andreas Fault at Parkfield, California" *(In Preparation for submission to Bulletin of the Seismological Society of America or GSA Bulletin in 2009)*

Toke, N.A. and J R. Arrowsmith "Multi-temporal scale tectonic geomorphology and fault zone structure of the Parkfield segment using LiDAR." *(in progress; for submission to Geomorphology, GSA Bulletin, or JGR in 2010)*

Ph.D. Dissertation Toké, Nathan A. "Interactions between Geologic Processes and Society: Earthquakes and Urban Landscape Modification" Arizona State University. *(Projected completion in summer 2010)*

Poster and Oral Presentations

Toké, N.A., J R. Arrowsmith, M. Rymer, A. Landgraf, J. Coyan, M. Busch, D. Haddad (2009). "Long-lived creep, M6 earthquakes, and a Holocene slip rate for the main trace of the San Andreas Fault at Parkfield, California" Annual Southern California Earthquake Center meeting, September 12-16th, 2009, Palm Springs, CA.

Toké, N.A., J R. Arrowsmith, M. Rymer, A. Landgraf, J. Coyan, M. Busch, D. Haddad (2008). "Paleoseismic interpretation and a preliminary geologic slip rate for the Parkfield segment of the San Andreas Fault", *Eos Trans. AGU, 89(52), Fall Meet. Suppl., Abstract T41A-1955.*

Toké, N.A. "Earthquake History of the Central San Andreas Fault (SAF): Paleoseismology, slip budget analysis, and implications for fault zone structure and seismic hazard." *Universidad de Granada, Spain; Conferencia May 30th, 2008.*

Toké, N.A., and Arrowsmith, J R., (2007). "Paleoseismic and Holocene slip rate investigations along the San Andreas Fault, at Parkfield, California": *Eos Trans. AGU, 88 (52), Fall Meet. Suppl., Abstract T43A-1097.*

Toké, N.A. "Fresh from the field: Investigation of Holocene slip rate along the Parkfield segment of the San Andreas Fault" *Arizona State University, School of Earth and Space Exploration Graduate Research Seminar, November 5th, 2008.*

Arrowsmith J R., Structural geology, tectonic geomorphology, and recent slip history of the south-central San Andreas Fault, *Geological Society of America Annual meeting*, Paper No. 155-3, 2007. Invited Pardee Symposium presentation. About 30% of the presentation covered portions of these results.

Toké, N.A., and Arrowsmith, J R., (2007). "Fall 2007 Paleoseismic and Holocene slip rate investigations along the San Andreas Fault, at Parkfield, California", *SCEC Fall 2007 Annual Meeting.*

References

Arrowsmith, JR., K. McNally, and J. Davis (1997). Potential for Earthquake Rupture and M7 Earthquakes along the Parkfield, Cholame, and Carrizo Segments of the San Andreas Fault, *Seism. Res. Lett.* **68**, no. 6, 902-916.

Bevis, M., K. Hudnut, R. Sanchez, C. Toth, D. Grejner-Brzezinska, E. Kendrick, D. Caccamise, D. Raleigh, H. Zhou, S. Shan, W. Shindle, A. Yong, J. Harvry, A. Borsa, F. Ayoub, B. Elliot, R. Shrestha, B. Carter, M. Sartori, D. Phillips, F. Coloma, K. Stark, (2005), The B4 Project: Scanning the San Andreas and San Jacinto Fault Zones: *Eos Trans. AGU, 85(***47***), Fall Meet. Suppl., Abs. H34B-01*.

Bronk Ramsey C. 1995 Radiocarbon Calibration and Analysis of Stratigraphy: The OxCal Program *Radiocarbon* **37(2)** 425-430

Bronk Ramsey C., 2001, Development of the Radiocarbon Program OxCal, *Radiocarbon*, **43** (2A) 355-363

Bronk Ramsey, C., 2005. OxCal Program v 3.10

Crosby C.J. (2004). Digital database of faulting accompanying the 1966 Parkfield, California earthquake, *US Geol. Surv. Open File Report* **2004-1437**.

Harris, R.A. and R.J. Archuleta (1988). Slip Budget and potential for a M7 earthquake in Central California, *Geophy. Res. Lett.* **15**, 1215-1218.

Jennings, C. W., (1977). Geologic map of California, *California Division of Mines and Geology*, Geologic Data Map No. 2, scale 1:750,000

Lienkaemper, J. J., B. Baker, and F. S. McFarland (2006). Surface slip associated with the 2004 Parkfield California, earthquake measured on alinement arrays, *Bull. Seism. Soc. Am.* **96,** no. 4B, S239–S249.

Lienkamper, J.J. and W.H. Prescott (1989). Historic Surface Slip along the San Andreas Fault near Parkfield, California, *J. Geophy. Res.* **94**, 17647-17670.

Meade, B.J. and B.H. Hager (2005). Block models of crustal motion in southern California constrained by GPS measurements. *J. Geophys. Res.* **110**. B03403.

Murray, J., P. Segall, P. Cervelli, W. Prescott, J. Svarc (2001). Inversion of GPS Data for Spatially Variable Slip-rate on the San Andreas Fault near Parkfield, CA, *Geophy. Res. Lett.* **28**, 359-362.

Murray, J., and J. Langbein (2006). Slip on the San Andreas fault at Parkfield over two earthquake cycles and the implications for seismic hazard,*Bull. Seism. Soc. Am.* **96,** no. 4B, S283–S303.

Noriega, G. R., J R. Arrowsmith, L. B. Grant, and J. J. Young (2006). Stream channel offset and Late Holocene slip rate of the San Andreas fault at the Van Matre Ranch site, Carrizo Plain, California, *Bull. Seism. Soc. Am.* **96,** no. 1, 33–47.

Platt, J.P. and T.W. Becker, (2009) Where is the true transform boundary in California? *Annual Southern California Earthquake Center meeting*, September 12-16th, 2009, Palm Springs, CA.

Reimer PJ, MGL Baillie, E Bard, A Bayliss, JW Beck, C Bertrand, PG Blackwell, CE Buck, G Burr, KB Cutler, PE Damon, RL Edwards, RG Fairbanks, M Friedrich, TP Guilderson, KA Hughen, B Kromer, FG McCormac, S Manning, C Bronk Ramsey, RW Reimer, S Remmele, JR Southon, M Stuiver, S Talamo, FW Taylor, J van der Plicht, and CE Weyhenmeyer. 2004 *Radiocarbon* 46:1029-1058.

Rymer, M. J., J. C. Tinsley, J. A. Treiman, J R. Arrowsmith, K. B. Clahan, A. M. Rosinski, W. A. Bryant, H. A. Snyder, G. S. Fuis, N. Toke, and G. W. Bawden, (2006). Surface fault slip associated with the Parkfield, California, Earthquake, *Bull. Seism. Soc. Am.* **96,** no. 4B, S11–S27.

Segall, P. and R. Harris (1986). Slip Deficit on the San Andreas Fault at Parkfield, California, as Revealed by Inversion of Geodetic Data, *Science* **233**, no. 4771.

Sieh, K.E., (1978a). Central California Foreshocks of the Great 1857 Earthquake, *Bull. Seism. Soc. Am.* **68**, 1731-1749.

Sieh, K.E. (1978b). Slip along the San Andreas Fault associated with the great 1857 earthquake, *Bull. Seism. Soc. Am.* **68**, 1421-1448.

Sieh, K.E. and R.H. Jahns (1984). Holocene activity of the San Andreas fault at Wallace Creek, California, *Geol. Soc Am. Bull.* **95**, p. 883-896.

Sims, J.D., (1987). Late Holocene slip rate along the San Andreas Fault near Cholame, California, *Geol. Soc. Am. Abs.* 451.

Stuiver, M. and H.A. Polach (1977). Discussion: Reporting of 14C data, *Radiocarbon* **19**, 355-63.

Titus, S.J., C. DeMets, B. Tikoff (2005). New slip rate estimates for the creeping segment of the San Andreas Fault, California, *Geology* **33**, no. 3, 205-208.

Titus, S. J., C. DeMets, and B. Tikoff (2006). Thirty-five-year creep rates for the creeping segment of the San Andreas fault and the effects of the 2004 Parkfield earthquake: constraints from alignment arrays, continuous GPS, and creepmeters, *Bull. Seism. Soc. Am.* **96,** no. 4B, S250–S268.

Toke, N.A. and J R. Arrowsmith (2006). "Reassessment of a Slip Budget along the Parkfield segment of the San Andreas Fault" *Bull. Seism. Soc. Am.* **96**, no. 4B, pp. S339–S348,

Toke, N.A., J R. Arrowsmith, J.J. Young, and C.J. Crosby (2006). "Paleoseismic and Postseismic Observations of Surface Slip along the Parkfield Segment of the San Andreas Fault." *Bull. Seism. Soc. Am.*, **96** no. 4B, pp. S221–S238.

Table 1. Radiocarbon data arranged in stratigraphic order (figure 4 and Toke et al., 2006). Pretreatment and analyses were performed by either the NSF-Arizona AMS facility at the University of Arizona (AA-#) or the KECK University of California Irvine AMS Facility (UCI-#). These facilities use the background correction of Stuiver and Polach, (1977).

Sample ID[1]	NSF-AMS#	Sample Description	Stratigraphic Unit[2]	Fraction Modern	+/- [3]	^{14}C age (years BP)	+/-[4]	2σ calibrated age (cal A.D. / B.C.)[5]	Modeled and Trimmed 2σ calibrated age (cal A.D. / B.C.)[6]
(2) 04MST-33	AA-61393 UCI-49998	charcoal	between MSW-103 and MSW-104 (laminated silt/clay)	0.7044 0.7548	0.0033 0.0011	2815 (detrital) 2260	37 15	400-350 B.C. (53.4 %) 290-230 B.C. (42.0%)	400-350 B.C. (53.4 %) 290-230 B.C. (42.0%)
(2) 04MST-9	AA-61386 UCI-49993	charcoal	between MSE-102 and MSE-103 (laminated Silt/clay)	0.7563 0.7544	0.0034 0.0011	2243 2265	36 15	400-350 B.C. (57.5%) 290-230 B.C. (37.9%)	400-350 B.C. (57.5%) 290-230 B.C. (37.9%)
07MST-P1	*UCI-49992*	*charcoal piece*	*MSE-103 (massive clayey silt)*	*0.7445*	*0.0010*	*2370*	*15*	*510-430 B.C. (23.8%) 420-390 B.C. (71.6%)*	*Detrital*
04MST-6	*UCI-49552*	*charcoal*	*MSE-103 (massive clayey silt)*	*0.7438*	*0.0015*	*2375*	*20*	*520-390 B.C.*	*Detrital*
04MST-18	UCI-49994	charcoal	lower charcoal stringer within MSE-108 (dark clay)	0.8790	0.0028	1035	30	890-920 A.D. (5.6%) 940-1040 A.D. (89.8%)	890-920 A.D. (6.7%) 940-1040 A.D. (88.7%)
04MST-17	*AA-61387*	*charcoal*	*MSE-110 (buried organic horizon)*	*0.8508*	*0.0037*	*1298*	*35*	*650-780 A.D.*	*Detrital*
04MST-26	*AA-61390*	*charcoal*	*MSE-110 (clayey silt)*	*0.7867*	*0.0035*	*1927*	*36*	*20-10 B.C. (1.0%) 0-140 A.D. (90.1%) 150-180 A.D. (2.3%) 190-220 A.D. (2.0%)*	*Detrital*
04MST-27	UCI-49996	charcoal	between MSE-110 and MSE-111 (clayey silt)	0.9430	0.0025	470	25	1410-1450 A.D.	1410-1450 A.D.
04MST-21	*UCI-49566*	*charcoal*	*MSE-112 (silty clay)*	*0.8663*	*0.0038*	*1155*	*40*	*770-980 A.D.*	*Detrital*
07MST-9	*UCI-49565*	*charcoal*	*MSE-112 (silty clay)*	*0.9186*	*0.0072*	*680*	*70*	*1220-1410 A.D.*	*Detrital*
04MST-22	*AA-61388*	*charcoal*	*MSE-112 (silty clay)*	*0.9221*	*0.004*	*652*	*35*	*1270-1330 A.D. (44.7%) 1340-1400 A.D. (50.7%)*	*Detrital*
04MST-3	UCI-49551	charcoal	MSE-112 (silty clay)	0.9493	0.0019	420	20	1430-1490 A.D.	1430-1460 A.D.
04MST-24	*AA-61389*	*charcoal*	*MSE-114 (laminated silt)*	*0.8311*	*0.0056*	*1486*	*55*	*1160-1300 A.D.*	*Detrital*
04MST-25	UCI-49554	charcoal	between MSE-114 and MSE-115 (laminated silt)	0.9485	0.0021	425	20	1430-1485 A.D.	1440-1470 A.D.
04MST-28	*UCI-49555*	*charcoal*	*top of MSE-115 (laminated silt/clay)*	*0.9287*	*0.0019*	*595*	*20*	*1300-1370 A.D. (72.2%) 1380-1410 A.D. (23.2%)*	*Detrital*
04MST-29	UCI-49997	charcoal	within MSE-115 (silty sand)	0.9488	0.0016	420	15	1435-1480 A.D.	1440-1480 A.D.
07MST-8	UCI-49564	charcoal	between MSE-117 and MSE-118 (silty sand)	0.9486	0.040	425	35	1410-1530 A.D. (86.2%) 1590-1620 A.D. (9.2%)	1440-1530 A.D. (91.0%) 1590-1620 A.D. (4.4%)
04MST-16	UCI-49553	charcoal piece	MSW-106 (clayey sand)	0.9545	0.0019	375	20	1440-1530 A.D. (67.6%) 1570-1630 A.D. (27.8%)	1440-1530 A.D. (67.6%) 1570-1630 A.D. (27.8%)
04MST-32	*AA61392*	*charcoal*	*MSE-118 (sandy clay)*	*0.7833*	*0.0049*	*1961*	*51*	*100 B.C.-140 A.D.*	*Detrital*
04MST-30	*AA61391*	*charcoal*	*MSE-119 (silty clay)*	*0.9558*	*0.0041*	*363*	*34*	*1440-1640 A.D.*	*Detrital*
04MST-31	UCI-49556	charcoal	MSE-119 (silty clay)	0.9761	0.0020	195	20	1650-1690 A.D. (22.2%) 1730-1810 A.D. (53.3%) 1930-1960 A.D. (20.9%)	1650-1690 A.D. (22.3%) 1730-1810 A.D. (52.3%) 1930-1960 A.D. (20.8%)

(1) Assigned sample name based upon: A) the year collected, B) the trench of collection, and C) the order of collection
(2) Stratigraphic unit: Trench name, east or west stratigraphy, higher numbers are younger layers. 2004 and 2007 units are correlative, but with different names: MSE-119 here is equivalent to MSE-24 in 2004; MSW-106 here is equivalent to MSW-7 in 2004; MSE-108 is equivalent to MSE 6/7 in 2004; MSE 5 from 2004 is subdivided to MSE 105-107; MSE 8 from 2004 is equivalent to MSE 109-110 here. For further explanation see Toke et al., 2006 and the forthcoming Toke et al., in preparation supplemental online material.
(3) Error value (2σ) assessed in the calculation of the modern fraction.
(4) Error value (2σ) assessed in the calculation of ^{14}C years before present.
(5) Determined using single samples in OxCal 3.10 (Bronk Ramsey, 1995; 2001; and 2005) and using the atmospheric data of Reimer et al., (2004).
(6) Same as (5), but sequenced, modeled, and trimmed in OxCal v3.10 after *removal of detrital samples*.

Table 2. Radiocarbon data from PT paleoseismic trenches. Arranged by relative stratigraphic age (Figure5 and Toke et al., 2006). Pretreatment and analyses were performed by either the NSF-Arizona AMS facility at the University of Arizona (AA-#) or the KECK University of California Irvine AMS Facility (UCI-#). These facilities use the background correction of Stuiver and Polach, (1977).

Sample ID[1]	NSF-AMS#	Sample Description	Stratigraphic Unit[2]	Fraction Modern	+/- [3]	^{14}C age (years BP)	+/-[4]	2σ calibrated age (cal A.D. / B.C.)[5]	Modeled and Trimmed 2σ calibrated age (cal A.D. / B.C.)[6]
07PT-SE14	UCI- 49563	charcoal	PTE-033 (thin laminated silt/clay)	0.6498	0.0013	3460	20	1880-1730 B.C (87.6%) 1720-1690 B.C. (7.8%)	1880-1730 B.C. (87.7%) 1720-1690 B.C. (7.7%)
04PT-7	*AA-61382*	*charcoal*	*PTE-037 (thin laminated silt/clay)*	*0.6018*	*0.0029*	*4079*	*39*	*2870-2800 B.C. (16.3%)* *2760-2480 B.C (79.1%)*	*Detrital*
(2) 07PT-NW9	UCI-49991 UCI-49560	charcoal	PTE-040 (clayey sand)	0.6884 0.6891	0.0009 0.0016	3000 2990	15 20	1310-1190 B.C. (91.2%) 1180-1160 B.C (1.5%) 1150-1130 B.C. (2.7%)	1320-1190 B.C. (92.3%) 1180-1160 B.C. (1.1%) 1150-1130 B.C. (2.0%)
04PT-3	*AA-61381*	*charcoal single piece*	*PTE-042 (thin laminated silt/clay)*	*0.6677*	*0.0033*	*3244*	*40*	*1620-1430 B.C.*	*Detrital*
(2) 04PT-8	*AA-61383* *UCI-49990*	*charcoal single piece*	*PTE-043 (clayey silt)*	*0.6993* *0.6940*	*0.0032* *0.0009*	*2873* *2935*	*37* *15*	*1210-1040 B.C.*	*Detrital*
07PT-NW2	*UCI-49558*	*charcoal*	*PTE-043 (light grey silt/clay)*	*0.7007*	*0.0016*	*2855*	*20*	*1120-970 B.C. (86.5%)* *960-930 B.C. (8.9%)*	*Detrital*
04PT-1	UCI-49989	charcoal	PTE-043 (clayey silt)	0.7299	0.0012	2530	15	800-530 B.C	810-660 B.C.
07PT-NW-1	UCI-49557	charcoal	PTE-047 (near boundary with sandy unit and C-horizon)	0.7293	0.0017	2535	20	800-740 B.C. (41.0%) 690-660 B.C (22.0%) 650-550 B.C. (32.4%)	780-740 B.C. (5.2%) 690-660 B.C. (40.5%) 650-560 B.C. (49.8%)
07PT-NW-4	UCI-49559	charcoal	PTE-048g (light grey clay)	0.7297	0.0015	2530	20	790-740 B.C. (34.5%) 690-660 B.C. (21.7%) 650-540 B.C. (39.2 %)	690-660 B.C. (8.8%) 650-540 B.C. (86.6%)
07PT-SE12	UCI-49562	charcoal	PTFZ-010 (dark clay in FZ)	0.8475	0.0017	1330	20	650-710 A.D. (85.7%) 740-770 A.D. (9.7%)	650-710 A.D. (87.4%) 740-770 A.D. (8.0%)
07PT-NW16	UCI-49561	charcoal	PTW-096 (clayey sand)	0.8465	0.0019	1340	20	640-700 A.D. (91.5%) 750-770 A.D. (3.9%)	640-700 A.D. (91.5%) 750-770 A.D. (3.9%)
04PT-13	AA-61384	Charcoal	PTFZ-005 (thin layer of leaf and other organic matter)	0.916	0.0039	705	35	1250-1320 A.D. (74.1%) 1350-1390 A.D. (21.3%)	1250-1320 A.D. (71.5%) 1350-1390 A.D. (23.9%)

(1) Assigned sample number based upon: A) the year collected, B) the trench of collection, and C) the order of collection.
(2) Stratigraphic unit: Trench name, east or west stratigraphy, higher numbers are younger layers. Units are correlative between 2007 and 2004 trenches however the unit names have been changed: Here PTW-096 is equivalent to PTW 5; PTE-039 is correlative to PTE 11; and PTE-048 is correlative to PTE 1.
(3) Error value (2σ) assessed in the calculation of the modern fraction.
(4) Error value (2σ) assessed in the calculation of ^{14}C years before present.
(5) Determined using single samples in OxCal v3.10 using the atmospheric data of Stuiver et al., (1998).
(6) Same as (5), but sequenced, trimmed, and modeled in OxCal v3.10 without clearly detrital samples.

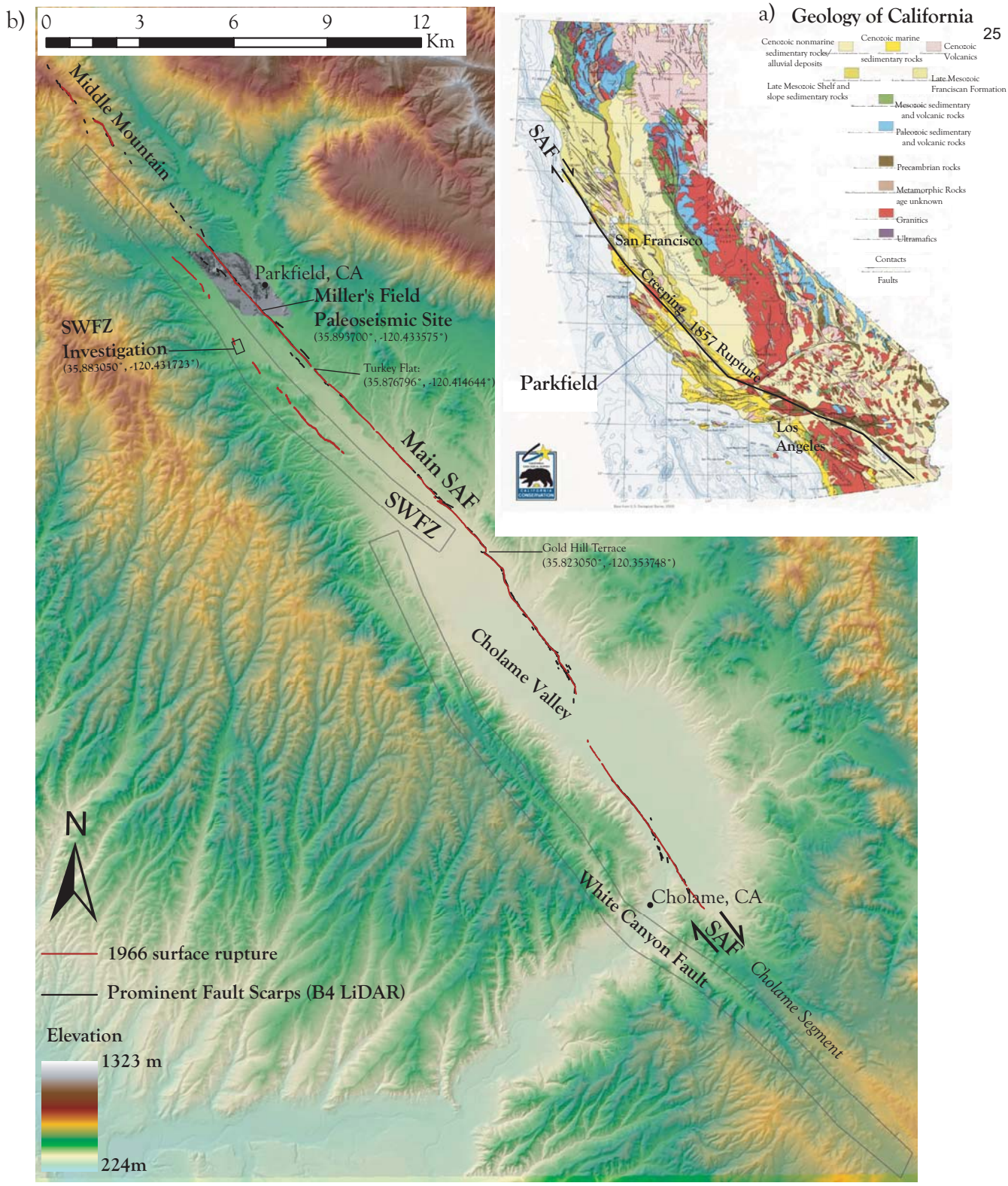

Figure 1 a) The Parkfield segment of the SAF is located between a creeping section of the SAF to the NW and segments to the SE which last slipped in the great 1857 Fort Tejon Earthquake (Sieh, 1978a,b; Geologic Map of California: Jennings, 1977). b) The Parkfield segment has ruptured in 6 historical moderate magnitude earthquakes such as the 1966 rupture (red lines; Crosby 2004) and slips via aseismic fault creep which decreases from ~25mm/yr at Middle Mountain in the NW to nearly zero near the town of Cholame, CA (e.g., Murray and Langbein, 2006). Mapping of tectonic geomorphology (Toke and Arrowsmith, in progress) shows that historical surface ruptures do not exactly coincide with prominent fault scarps (black). In addition to the main SAF, the SWFZ and other smaller faults have slipped in the most recent historical earthquakes (e.g., Rymer et al., 2006). The White Canyon Fault displays a prominent tectonic signal in the above Hillshade imagery and is parallel to the SAF with a separation distance of less than 3 km in the Parkfield segment and less than 1 km on the NW Cholame segment. The Miller's Field Paleoseismic site (figures 3-7) is located just south of the town of Parkfield, CA. The SWFZ investigation of the Ranchita Canyon Fan was located about 1 km west of the Miller's Field site (figure 2).

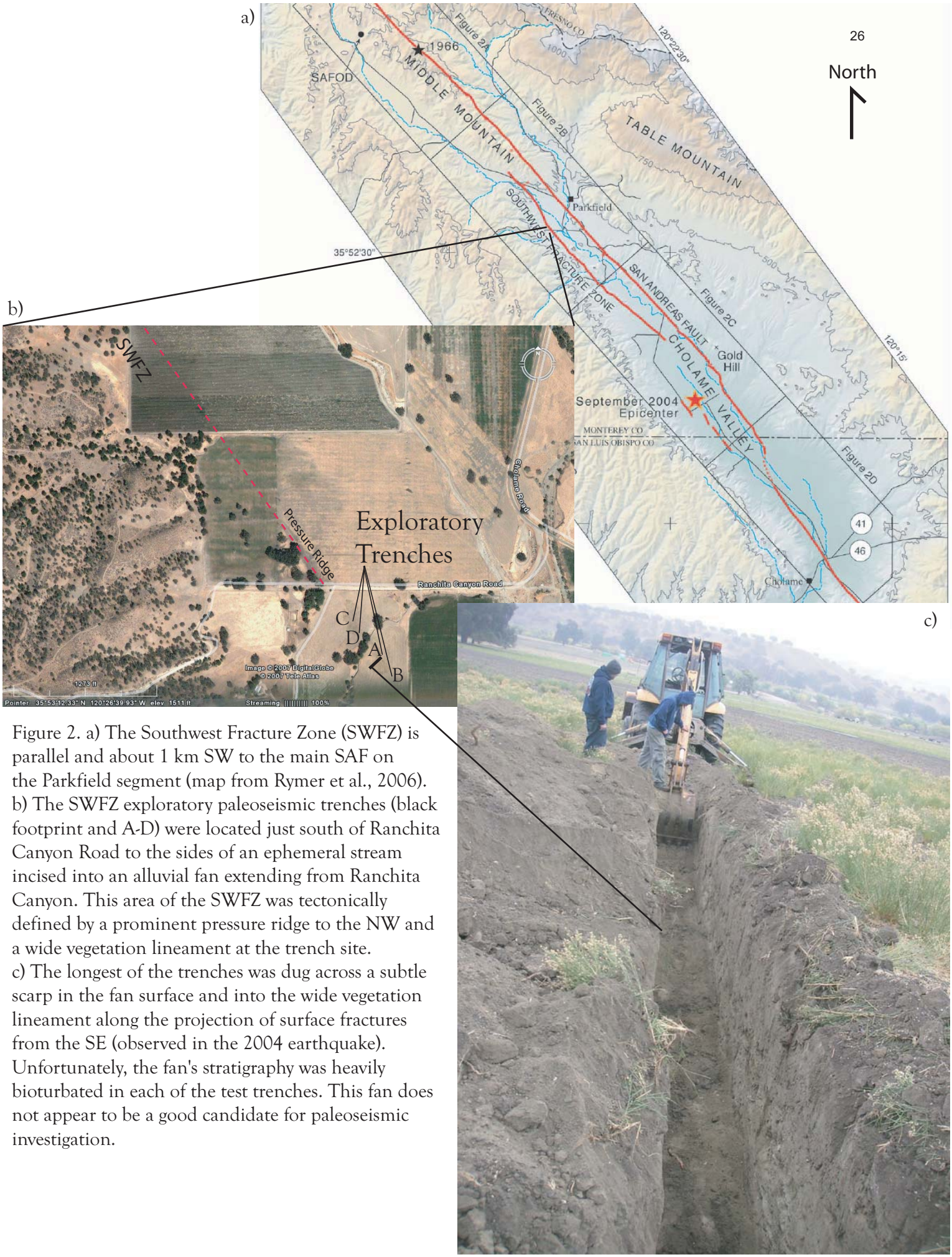

Figure 2. a) The Southwest Fracture Zone (SWFZ) is parallel and about 1 km SW to the main SAF on the Parkfield segment (map from Rymer et al., 2006). b) The SWFZ exploratory paleoseismic trenches (black footprint and A-D) were located just south of Ranchita Canyon Road to the sides of an ephemeral stream incised into an alluvial fan extending from Ranchita Canyon. This area of the SWFZ was tectonically defined by a prominent pressure ridge to the NW and a wide vegetation lineament at the trench site. c) The longest of the trenches was dug across a subtle scarp in the fan surface and into the wide vegetation lineament along the projection of surface fractures from the SE (observed in the 2004 earthquake). Unfortunately, the fan's stratigraphy was heavily bioturbated in each of the test trenches. This fan does not appear to be a good candidate for paleoseismic investigation.

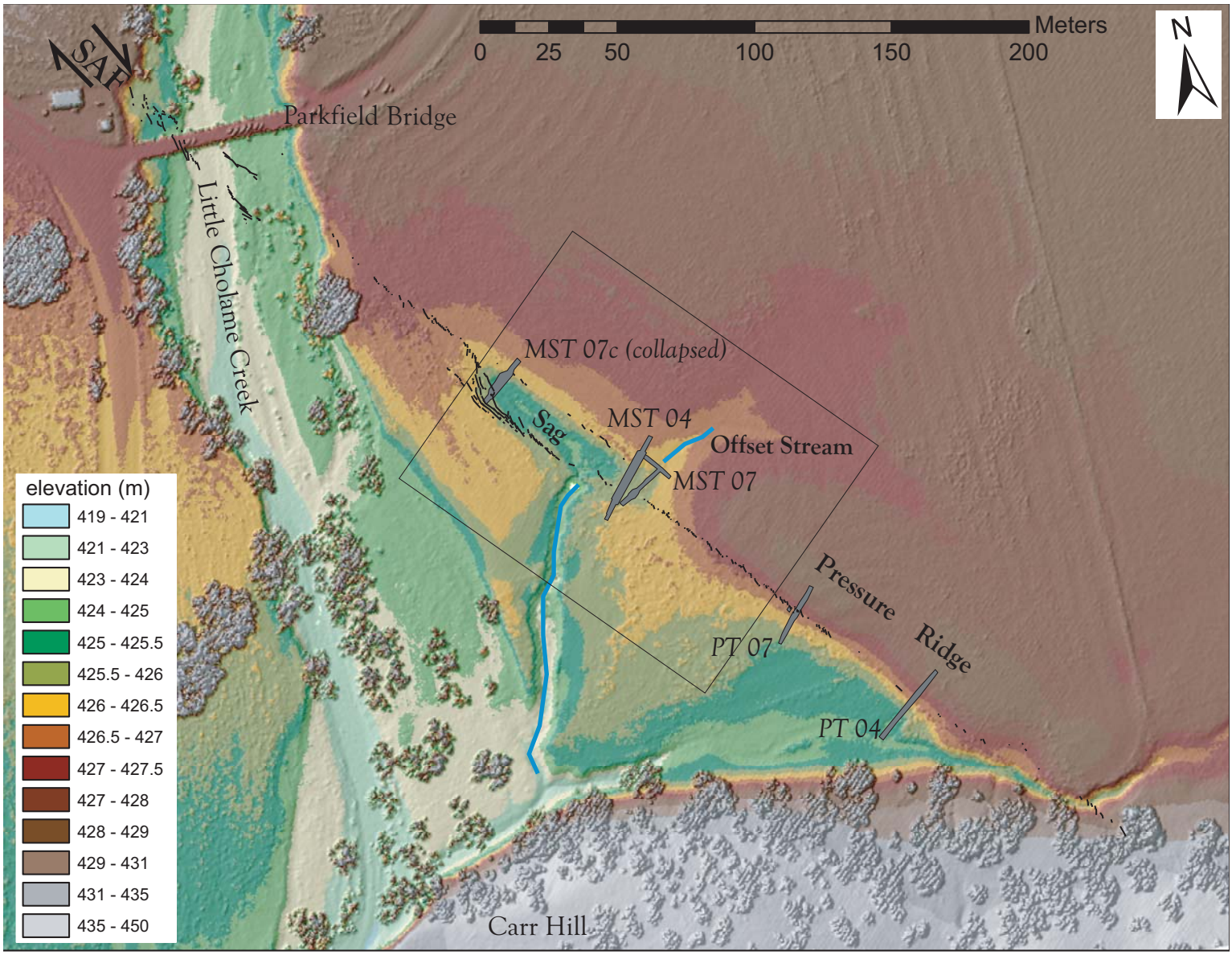

Figure 3. The Miller's Field paleoseismic site is a tectonically deformed fluvial terrace of the Little Cholame Creek. The Little Cholame Creek flows from the east side of Middle Mountain (figure 1) to the Cholame Valley in the South. Prior to the 2004 Parkfield earthquake we opened two paleoseismic trenches at this site (MST 04 and PT 04; Toke et al., 2006). After completing our 2004 investigations, the M6 Parkfield earthquake occurred. We visited the Miller's Field 2 and 3 days following the earthquake and documented the surface deformation at the site (black lines). The 2004 rupture depicts the shallow structure of the SAF at this site. A right step in the right-lateral SAF has resulted in tension and the formation of a sag pond on the terrace. Additionally, to the SE the SAF bends left at Carr Hill helping to form the pressure ridge on the NE side of the SAF. We located 3 of our 2007 trenches at the Miller's Sag. One trench (MST 07 c) was located at the NW end of the sag pond where the most vertical offset was seen in the 2004 rupture, unfortunately the Miller's Field Site was so wet in 2007 that we could not keep up with pumping water out of all the trenches at once and MST 07c collapsed. At the SE end of the sag we opened both a fault normal and fault parallel trench (MST 07; figure 4 and MST 07parallel). The parallel trench was opened to test if the upstream side of the small right-laterally offset stream (blue line) was associated with any channel deposits. In addition we opened a pressure ridge trench (PT 07; figure 5). These trenches were opened to test for consistency of interpretation with the 2004 investigation and to collect more radiocarbon samples for age control and measurement of a slip rate for the main trace of the SAF (figure 6; black box and figure 7).

a) 2007 Miller Sag Trench, southeast wall (MST07se)

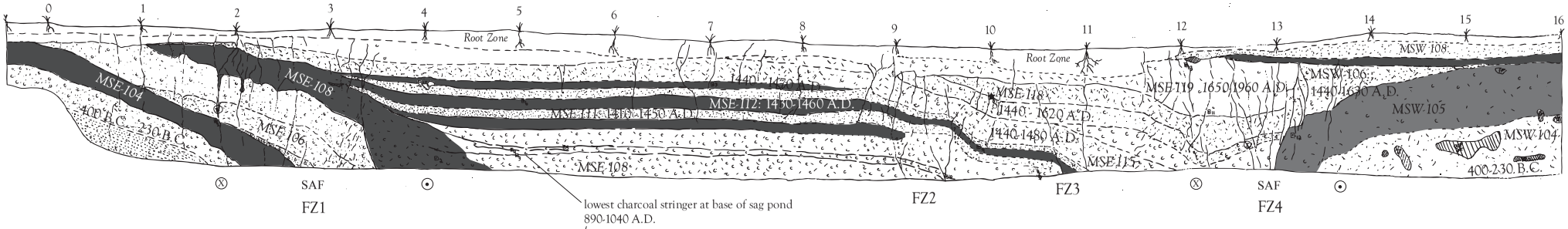

lowest charcoal stringer at base of sag pond
890-1040 A.D.

b) 2007 Miller Sag Trench, southeast photolog mosaic

c) 2007 Miller Sag Trench, northwest wall (MST07nw; flipped about the horizontal axis for comparison with MST07se)

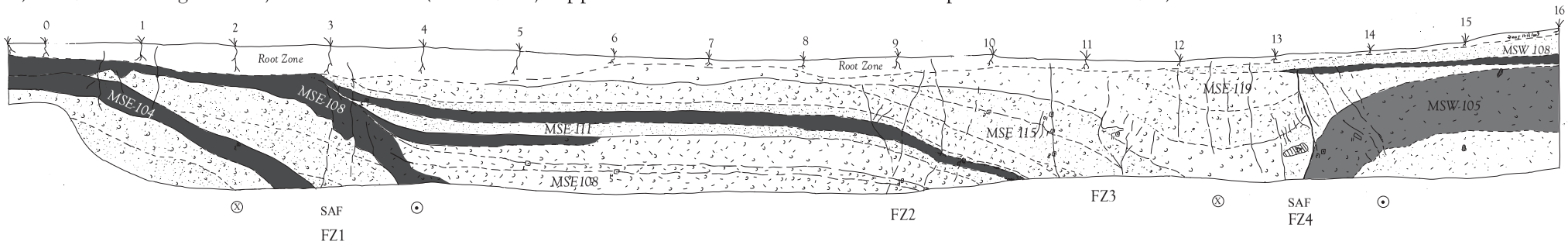

d) Explanation of logging

- clayey organic-rich soil horizon
- clay
- silt and clay
- clayey sand
- sand and silt
- sand
- gravels
- clay shear band (fault)
- radiocarbon age
- animal burrow
- contact

Figure 4. The 2007 Miller Sag Trenches exposed the same stratigraphic sequence as the 2004 MST trenches (Toke et al., 2006). However, the 2007 trenches revealed the stratigraphic relationship across fault zone 2 (FZ2) and provided additional radiocarbon samples. Here we plot a summary of the 2 sigma trimmed age ranges interpreted from all MST trenches (2004 and 2007) on the MST07se trench log (a). For detailed age ranges see Table 1. The MST07se photolog provides a visual references for our logging interpretations (b). Note the obliquity of the fault surfaces exposed between FZ3 and FZ4 in the photolog. The MST07nw trench (c) was drawn with considerably less deformation interpretation because it was difficult to discern the clay shear bands on the sun facing side of the trench. Stratigraphy consisted of a variety of terrace deposits and reworked sag material (d). For a detailed explanation of individual units see text and especially (Toke et al., 2006). Herein we do not show MST07parallel because it only displayed tabular beds of the overbank terrace deposits.

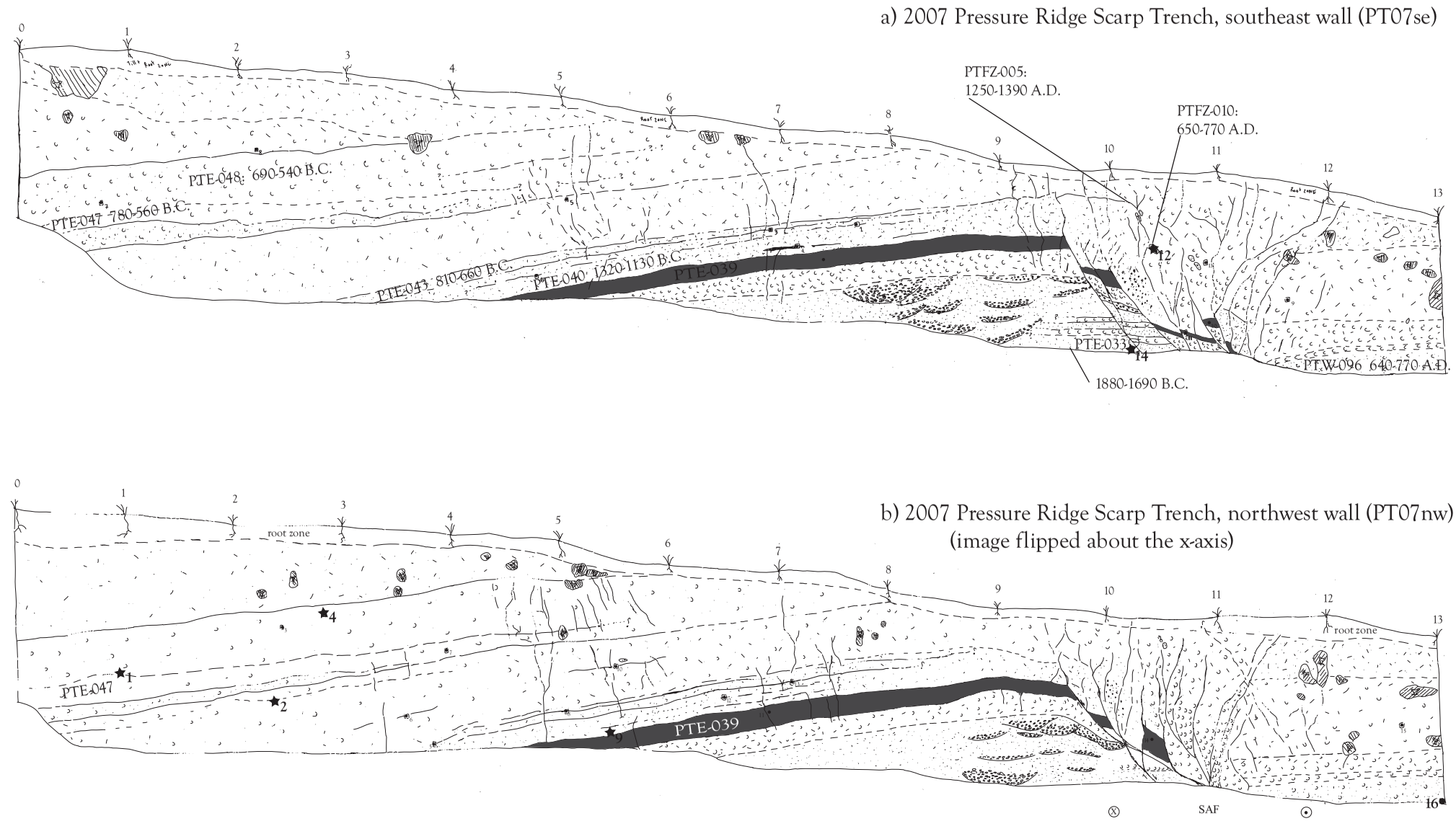

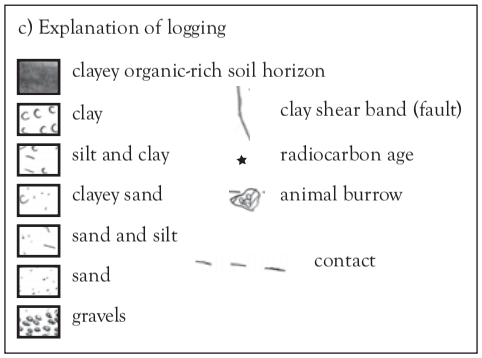

Figure 5. 2007 trench logs for the southeast (a) and northwest (b) walls of the Miller's Field pressure ridge trenches (PT07se and PT07nw; for location see figure 3. The stratigraphy displays apparent oblique right-lateral deformation of fluvial overbank deposits and buried soil horizons. Units and deformation features (c) are consistent with stratigraphy from PT04; for a correlative view the PT04 trench stratigraphy see text and Toke et al., 2006. In (a) we lable select stratigraphic units and provide the trimmed radiocarbon ages amalgamated from all samples analyzed in PT04 and PT07; for full explanation of radiocarbon see table 2.

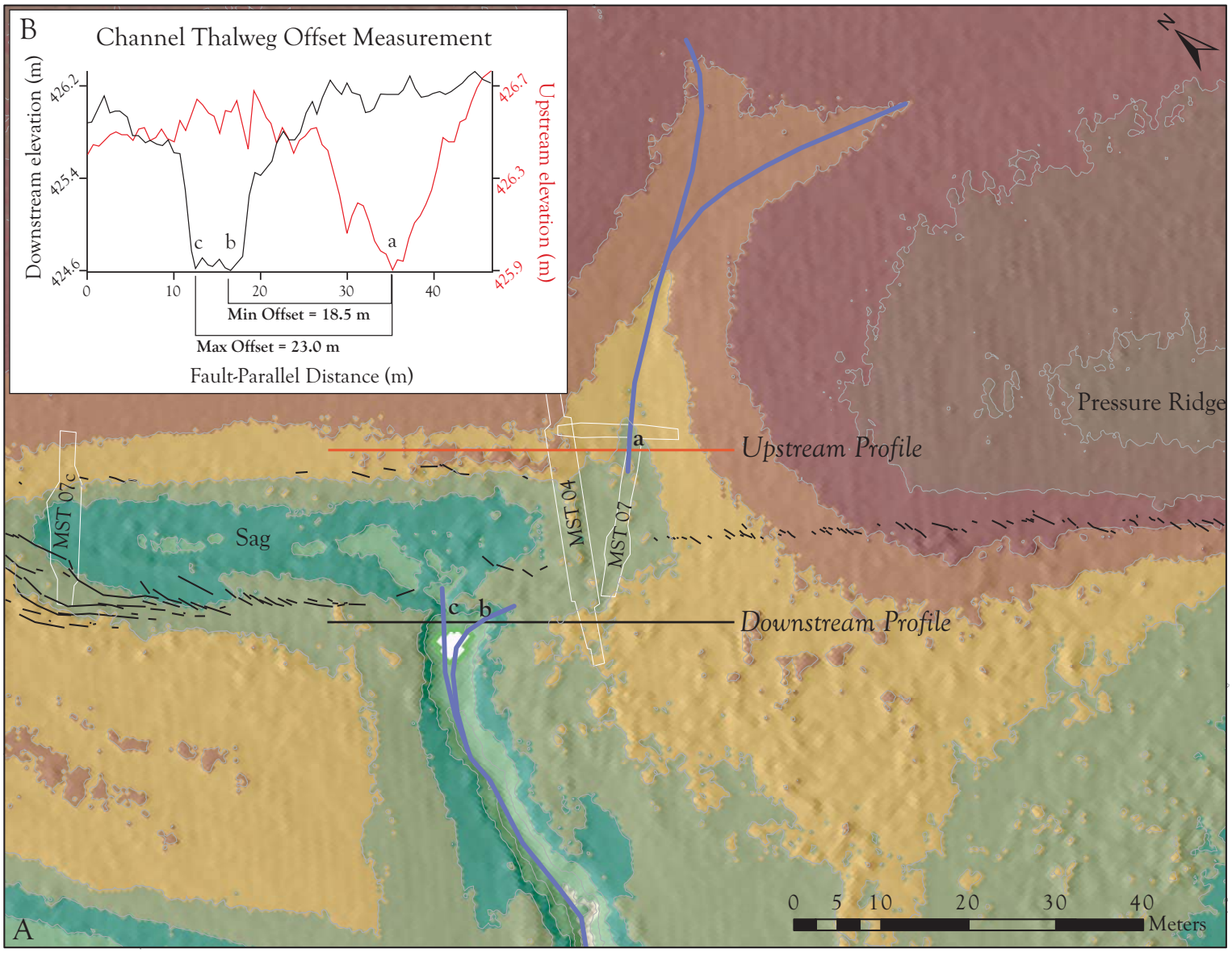

Figure 6. A) The Miller's Field (figure 3) sag pond contains a right-laterally offset channel. To the southwest of the fault (2004 rupture cracks shown in black) the channel is incised about 1 meter into the Little Cholame Creek fluvial terrace. Additionally, small steps within the channel's bed reveal channel gravels. On the northeast side of the fault the channel is only defined by a subtle incision into the terrace. The lower channel is an older beheaded channel that has been offset along the SAF. Incision of the upper channel was focused by beheaded channel as it was directly across the fault and the sag/pressure ridge scarp formed. Thus we use radiocarbon ages from the lower sag pond stratigraphy (figure 4; table 1) as a proxy for the age of incision of the upstream channel and estimate a late holocene slip rate for the main SAF trace at Parkfield (figure 7). In the field, we estimated about 20 m of right-lateral offset using a tape measure and the naked eye. B) To more precisely measure the offset we use a 0.5 m digital elevation model (DEM) created from the 2005 B4 LiDAR. From the LiDAR DEM we extracted upstream and downstream sag parallel topographic profiles to measure the right-lateral offset between channel thalwegs. The position of the downstream channel thalweg could be interpreted to be at either b or c. Thus, we estimate a minimum thalweg offset of 18.5 m and a maximum thalweg offset of 23.0 m (figure 7a).

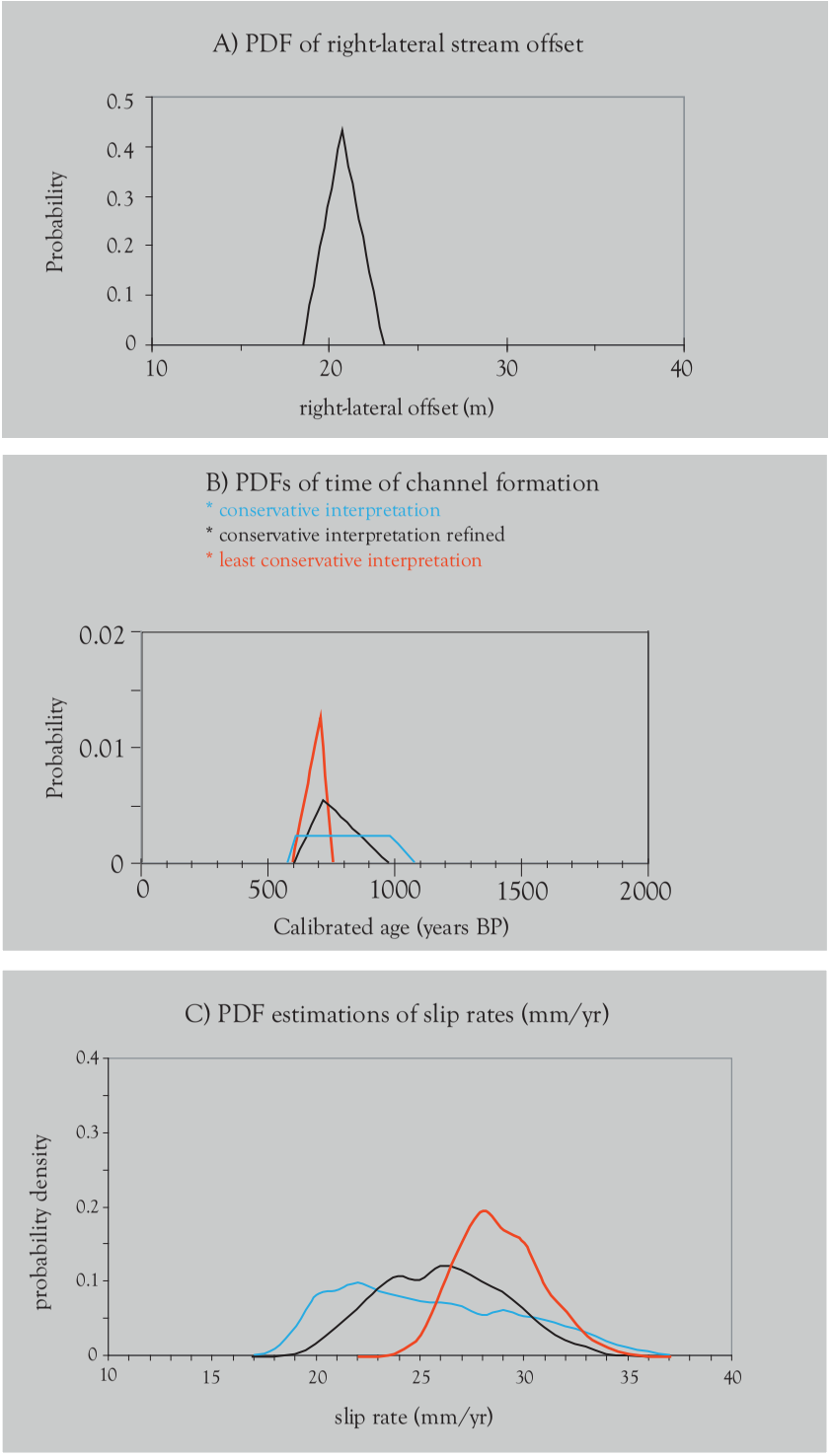

Figure 7. Probability Density Function (PDF) calculations of a late Holocene slip rate for the main SAF at Parkfield.

A) The maximum right-lateral offset of the Miller's Field sag pond channel (figure 6) is 23.0 m and the minimum is 18.5m. This PDF assumes equal probability and a median peak in probability at 20.8m.

B) Because the upstream portion of the offset channel is simply an incisional feature, we infer that it must have incised with the formation of the sag and uplift of the pressure ridge scarp. Moreover, the previously-beheaded downstream channel must have been directly across the fault to focus scarp erosion and therefore the channel talwegs are piercing points. We date this offset using the ages of the sag pond and scarp deposits (figures 4-5 and table 1-2) because they are a proxy for the age of incision. We present three possible PDFs for the time of channel formation based upon different assumptions about the relationship between channel incision and the age of scarp and sag pond deposits. The most conservative interpretation is the blue curve, we refine this conservative interpretation based upon the age of a scarp deposit preserved within the fault zone of the pressure ridge trenches (black curve). Finally, we use this same pressure ridge deposit to explore a more bold interpretation (red curve). See text for discussion of these age assumptions.

C) Slip rate PDFs are constructed by combining the PDFs of right-lateral offset and time of channel formation. The PDF colors correspond to the curves from part B. The most conservative interpretation of the age of channel incision results in a mean probability of 24.5 (+12/-7) mm/yr (blue curve). A more refined interpretation (black curve) suggests a slip rate of 26.1 (+8/-7) mm/yr. Finally, using a pressure ridge deposit to constrain the age of channel formation, the least conservativeslip rate estimate (red curve) suggests a mean probability of 28.8 (+6/-5) mm/yr. None of these ranges preclude a slip rate greater than 32 mm/yr, however the probability data are consistent with a slip rate of 25-30 mm/yr for the main trace of the SAF at Parkfield.